

Shear strength reduction factor used in critical state models with hardening

Isabella Maria Martins de Souza¹ , Daniela Toro Rojas^{1#} , Ana Carolina Gonzaga Pires¹ ,
Márcio Muniz de Farias¹ , Manoel Porfírio Cordão Neto¹ 

Article

Keywords

Shear strength reduction
Strength reduction factor
Critical state models
Safety factor

Abstract

The slope stability analyses are important to predict environmental, financial, and human life impacts. The Limit Equilibrium Method (LEM) is commonly used to estimate a slope's Safety Factor (*SF*). However, the Finite Element Method (FEM) is increasingly applied to slope stability analyses, using different approaches, among which the technique of Shear Strength Reduction (SSR) is commonly used in perfectly plastic elastic models. The objective of this study is to present a discussion about these two methodologies, using critical state models with or without hardening will be used to model the stress-strain behavior of the soil mass. The results obtained in the case study presented, using LEM and FEM considering critical state models with and without hardening are consistent and allowed verifying the stability condition of the slope. Also, the reduction factors are smaller when compared to the results using perfectly plastic elastic models.

1. Introduction

Geotechnical accidents involving natural slopes or large structures such as dams and embankment in general can seriously impact society. The failure of these structures can result in significant financial, environmental, and human losses. Therefore, verifying the stability condition of a slope is of utmost importance to prevent the occurrence of catastrophic accidents.

In general, slope failure is caused by processes that increase internal shear stresses, such as external loads and the removal of materials that provide support at the toe of slope. In addition, some factors may reduce the soil's shear strength, such as the increase of pore pressure and changes caused by weathering and physical-chemical activity.

There are several methods to analyze the stability of slopes, among them the methods based on the Limit Equilibrium Method (LEM). This method divides the slope into "n" slices, each subjected to a set of forces. However, it is necessary to formulate some hypotheses to make the problem determined. In addition, LEM makes some hypotheses that may compromise the accuracy of the response, such as the need to predefine a failure surface, stresses are determined only on the failure surface and between slices, the safety factor is the same for both friction and cohesion strength components, the same safety factor value is applied to all

slices, and the material is considered rigid and perfectly plastic (Fredlund & Rahardjo, 1993, 2012; Duncan et al., 2014).

The Finite Element Method (FEM), introduced by Clough & Woodward (1967), is also a commonly used tool for solving geotechnical problems and can be applied to verify the stability condition and estimate the safety factor of a structure. The FEM consists of discretizing the soil mass into regions called finite elements, which are interconnected by common nodes. This method calculates displacements, pore pressures, and other variables in each finite element and, thus, allows for solving geotechnical problems with more accuracy, such as the stability of slopes and settlement of foundations, among others (Dong et al., 2018).

The Finite Element Method can be used to analyze slope stability in two ways. The first one was proposed by Matsui & San (1992), and it is defined as the Shear Strength Reduction Method (SSR), which is the method used in this work. The second was proposed by Farias & Naylor (1998) and is called the Improved Limit Equilibrium Method. The later performs an analysis similar to the conventional Limit Equilibrium Method, however, the stresses along the failure surface are calculated from the stress and pore pressure fields arising from a finite element analysis.

The Shear Strength Reduction Method (SSR), introduced by Matsui & San (1992), can also be applied to verify the safety of a geotechnical structure. Numerically, SSR alters the shear strength parameters by repeatedly

[#]Corresponding author. E-mail address: dtr1593@gmail.com

¹Universidade de Brasília, Programa de Pós-graduação em Geotecnia, Brasília, DF, Brasil.

Submitted on January April 27, 2023; Final Acceptance on October 25, 2023; Discussion open until February 28, 2024.

<https://doi.org/10.28927/SR.2023.004123>



This is an Open Access article distributed under the terms of the Creative Commons Attribution License, which permits unrestricted use, distribution, and reproduction in any medium, provided the original work is properly cited.

applying a Strength Reduction Factor (*SRF*) until a critical *SRF* is found. The SSR can be applied in a finite element analysis and the critical *SRF* can be defined when the problem solution does not converge or the occurrence of excessive displacements, indicating the beginning of failure (Vardon et al., 2017).

The SSR method is commonly employed together with elastic perfectly plastic (EPP) models. However, this paper presents a discussion of this method using critical state models with or without hardening.

2. SSR and Critical State Models

The use of Critical State Models (Roscoe et al., 1958) with hardening when applying the Shear Strength Reduction Method (SSR) will be discussed below. It should be noted that the term “hardening” will be used in the context of isotropic hardening and can refer to both the increase in the yield surface as well as its contraction (softening).

As already mentioned, SSR alters the shear strength parameters and results in changes in the stress-strain constitutive matrix, which is used in the formation of the stiffness matrix K_{ij} :

$$K_{ij} = \int B_{mi} D_{ml} B_{lj} dV \quad (1)$$

where D_{ml} is the stress-strain constitutive matrix, and B_{lj} a matrix relating displacement and strains.

Thus, any change in the constitutive matrix reflects changes in the system's stiffness matrix, as can be easily visualized in Equation 1. Static equilibrium with external forces is given by:

$$F_i = K_{ij} u_j \quad (2)$$

where K_{ij} is the stiffness matrix, u_j is the displacement vector, and F_i represents external forces.

If the stiffness matrix changes due to the application of the *SRF*, an imbalance will occur that will be corrected with displacement increases, without the boundary conditions and external forces being changed. An illustration of what happens can be seen in Figure 1, where two “load-displacement” curves with different stiffness are presented. It should be noted that the stiffness illustrated in the figure is that of the system and not of a single element.

In Figure 2, point A represents a stress state that was within the elastic zone before the application of *SRF*, and after, it is located outside the reduced yield surface and violates the consistency law. Therefore, in the case of elastic perfectly plastic models without hardening, the violation of the consistency law is compensated by the appearance of plastic deformations, during some stress return algorithm to ensure consistency.

The stress-strain constitutive matrix (D_{ij}^{ep}) for elastic perfectly plastic models is given by:

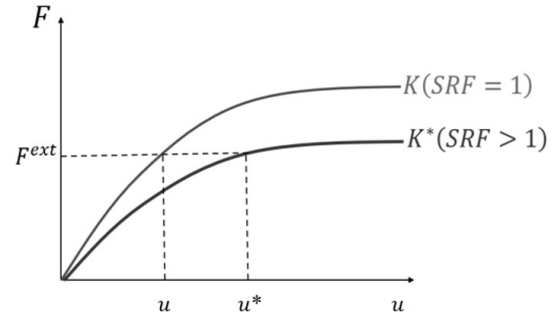


Figure 1. Effect of stiffness change due to *SRF* application, where K is the stiffness matrix for *SRF* equal to 1, K^* is the stiffness matrix for *SRF* less than 1, F^{ext} represents external forces, u is the initial displacement vector and u^* is the final displacement vector.

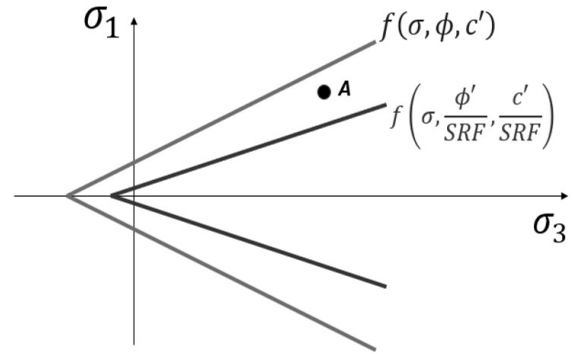


Figure 2. Yield surface before and after *SRF* application.

$$D_{ij}^{ep} = D_{ij}^e - \frac{(D_{im}^e b_m)(D_{jn}^e a_n)}{a_k D_{kl}^e b_l} \quad (3)$$

where D_{ij}^e is the elastic constitutive matrix, a_n is the vector normal to the yield function and b_m the normal to the plastic potential function. In models with associated flow rules, the plastic potential and the yield surfaces are the same, and therefore vector a_n and b_m are equal.

For points within the yield surface, the constitutive matrix is the elastic matrix D_{ij}^e . On the other hand, whenever a point touches or exceeds the plastic yield surface, the second term is activated and the constitutive matrix becomes D_{ij}^{ep} . In the case of these models, the matrix D_{ij}^{ep} always corresponds to a condition of lower stiffness than when the matrix D_{ij}^e is used.

Up to this point, the problem with using constitutive models that consider hardening is not evident. To illustrate the problem, Figure 3 will be used. Point A was located within the elastic region, but the consistency condition is violated after applying the reduction factor. However, for elastoplastic models that include hardening, such as critical state models, the matrix formulation is different.

In Figures 3 and 4, the yield surface (f) of the Modified Cam-Clay model is illustrate in the p' - q stress invariants

space. The yield surface in this case is an ellipsis with major axes at p_0 (called over-consolidation stress), and the minor axes is delimited the critical state failure criterion, given by a straight line with inclination M , related to the soil's friction angle at the critical state (CS). In critical state models, plastic deformations generate an increase in the yield surface, that is, hardening, which can be observed in Figure 4.

For the Modified Cam-Clay model the stiffness matrix expression is given by

$$D_{ij}^{ep} = D_{ij}^e - \frac{(D_{im}^e b_m)(D_{jn}^e a_n)}{a_k D_{kl}^e b_l + Y} \quad (4)$$

where the additional term Y is a scalar related to the model's hardening law and give by:

$$Y = \frac{\partial F}{\partial p_0} \frac{\partial p_0}{\partial \varepsilon_v^p} \frac{\partial F}{\partial p} \quad (5)$$

in which p_0 is over-consolidation stress (the stress-like internal hardening variable of the MMC model), ε_v^p is plastic volumetric strain (the strain-like internal hardening variable of the MMC model), and Y is the corresponding hardening modulus.

In this way, the application of the SSR generates at the same time a reduction of the friction strength parameter M and the variation of the state parameter related to the size of

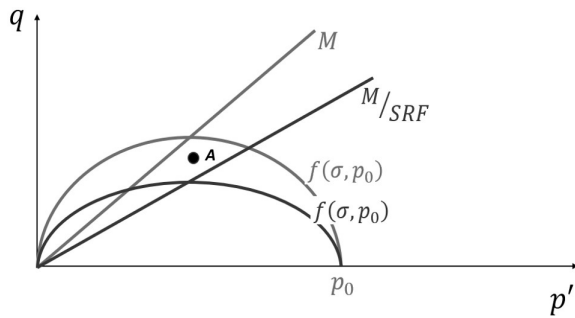


Figure 3. Effect of reduction factor in Cam-Clay type models.

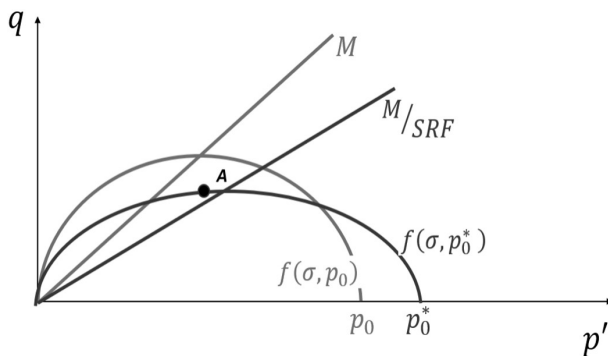


Figure 4. Evolution of the yield surface after SRF application.

the surface, p_0 . For the process to be considered similar to that described for elastic perfectly plastic models, the parameter p_0 must be constant or at least to have a small variation.

However, the hardening modulus tends to zero when the ratio $\eta = q/p$ tends to M . This occurs because the last term of Equation 5, $\partial F/\partial p$, tends to zero while the others do not depend on η . Additionally, for stress states near the failure surface the ratio η values are close to M , and therefore, Y values tend to zero. On the other hand, points that tend to have more significant hardening tend to be far from the failure surface (Figure 5).

For other models, such as Norsand (Jefferies, 1993; Jefferies & Shuttle, 2002; Cheng & Jefferies, 2020), the hardening modulus will also tend towards zero, even though the mathematical formulation may be different. Figure 6 shows the influence of the parameter M on the yield surface of the Norsand model, and it is easy to see that the statements proposed for the Modified Cam-Clay model are also valid for Norsand.

Therefore, considering that the effect of applying the reduction factor is to flatten the surface, one can imagine that the points most affected by the reduction factor are precisely those with an η value close to M . The region formed by these points will be the region of the formation of a potential failure surface. Points that would be subject to higher hardening would be those farther away from the “failure zone”.

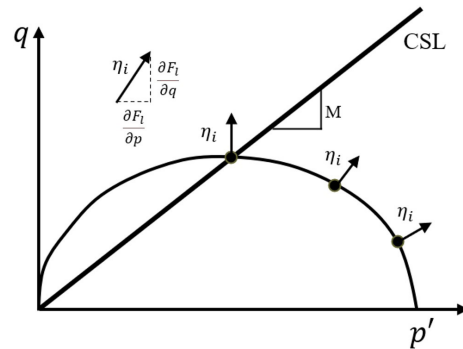


Figure 5. Surface normal vectors for different stress states.

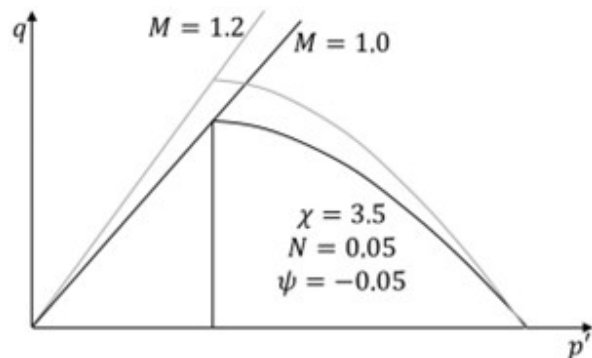


Figure 6. Effect of the MTC parameter on the yield surface of the Norsand model.

In the next items, it will be demonstrated how the reduction factor method can be used to evaluate the stability of geotechnical structures.

3. Application of the SSR

The case study in this work is a hypothetical natural slope representing highway slopes in Brasília, illustrated in Figure 7. The slope stability analysis will be carried out using two different methodologies, encoded in the SLOPE/W and SIGMA/W programs from GeoStudio (Geoslope International, Ltd, 2021). Initially, the Limit Equilibrium Method (LEM) will be applied using the Morgenstern-Price method to calculate the Factor of Safety (FS). Then, the Finite Element Method (FEM) will be employed using the shear strength reduction technique (SSR).

Furthermore, two constitutive models will be used to estimate the *SRF*: the elastic perfectly plastic model with Mohr-Coulomb failure criterion (MC) and the Modified Cam Clay (MCC). The first is a conventional model without hardening. The second is a critical state model that considers the isotropic hardening/softening of the flow surface (Roscoe et al., 1963, Roscoe & Burland, 1968).

The F.E. mesh consisted of 1722 quadrilateral elements with 4 nodes, with a length of 1 m on the face of the slope and 4 m elsewhere in the domain. Boundary conditions were applied that restricted only horizontal displacements on the sides and vertical displacements at the base of the geometry. The input data used is indicated in Table 1. It is worth noting that the values used in the Modified Cam Clay model and the Mohr-Coulomb failure criterion were obtained from triaxial tests carried out for a theoretical-experimental study of the behavior of tropical soils conducted by Futai (2002).

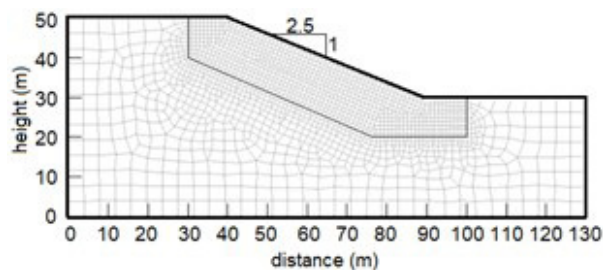


Figure 7. Case study geometry using the shear strength reduction (SSR) technique.

Using the Mohr-Coulomb failure criterion and the optimization of the SLOPE/W program to determine the critical failure surface, the safety factor value of 1.71 was obtained by the Limit Equilibrium Method. Figure 8 illustrates the failure surface resulting from this analysis.

In defining the critical *SRF* using the Mohr-Coulomb criterion, five points near the failure surface (P1 to P5) were monitored. Figure 9 illustrates the *xy* displacement for *SRF* values of 1.60 and 1.70. Figure 9a shows the slope on the verge of potential failure, as the monitored points exhibited displacements of more than 0.3 m. Figure 9b shows the potential failure zone, which is similar to the one obtained in the previously presented Limit Equilibrium Method.

Similar to the previous study, the aforementioned five points were also monitored in defining the critical *SRF* using the Modified Cam Clay model (MCC). Figure 10 illustrates the *xy* displacement for *SRF* values of 1.30 and 1.40. Figure 10a shows the structure on the verge of potential failure, as the monitored points exhibited displacements of more than 0.3 m. Figure 10b presents the formed failure surface.

The displacements at points P1 to P5 are presented in Figure 11 for a comparative analysis between the displacements of the five monitored points of the Modified Cam Clay model

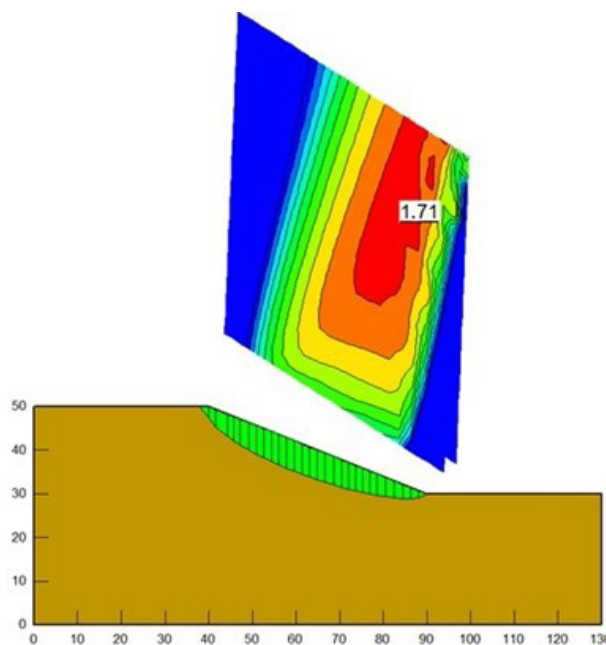


Figure 8. Result of LEM.

Table 1. Input data.

Constitutive model	γ (kN/m ³)	ν	E (MPa)	c (kPa)	ϕ (°)	e_i	κ	λ	M (initial)	OCR
Mohr-Coulomb	18	0.35	12	7	28	-	-	-	-	-
Modified Cam-Clay	18	0.35	-	-	-	0.80	0.02	0.17	1.14	1.20

Legend: see List of Symbols.

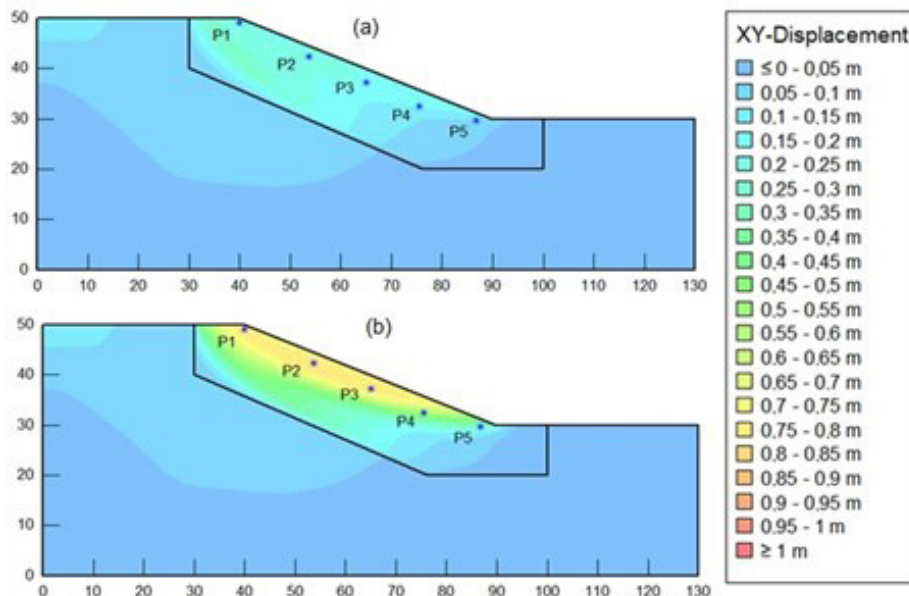


Figure 9. Result of the MC failure criterion, (a) *SRF* of 1.60 and (b) *SRF* of 1.70.

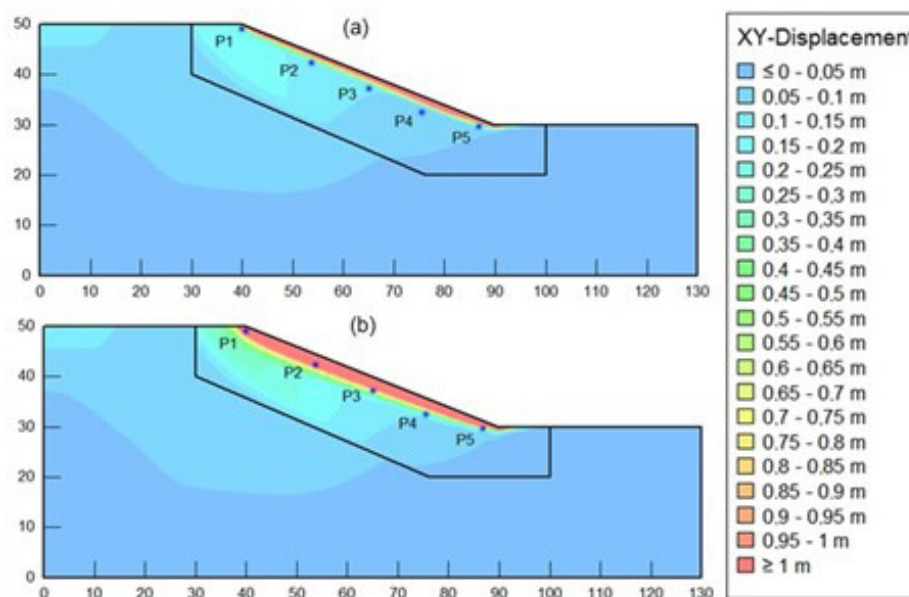


Figure 10. Result of the MCC model, (a) *SRF* of 1.30 and (b) *SRF* of 1.40.

(MCC) and the Mohr-Coulomb criterion (MC) as a function of the applied *SRF*. The curve in red corresponds to the average of the displacements of the five monitoring points.

The average displacement of the monitored points allowed for estimating the critical *SRF* between 1.60 and 1.70 for the MC model. At 1.60, the onset of slope instability in the analyzed slope can be inferred. For the second *SRF* value (1.70), a mean displacement of 1 m was found, representing a significant deformation of the structure of 5%. Similarly,

the average displacement of the monitored points using the MCC model allowed for estimating the critical *SRF* between 1.30 and 1.40.

In addition, considering the average displacement values of the monitored points, a complementary comparison was made to determine the critical *SRF*. Figure 12 illustrates the derivative of the curve of average displacement values of the monitored points as a function of the applied *SRF* for the two models used. The results observed in Figure 12 confirmed the

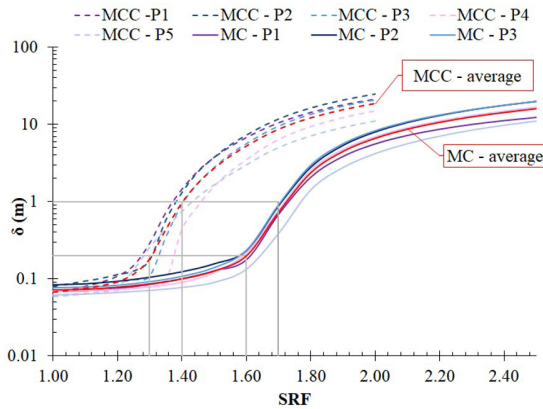


Figure 11. Comparison of the displacement (δ) between the MCC and MC models.

critical *SRF* value of 1.30 and 1.60 for the MCC and MC models, respectively. Furthermore, at these points, there is a significant increase in the displacements resulting from the applied *SRF*.

Another relevant point is the fact that the failure surface obtained by the MC criterion is different from the surface presented in the MCC model. The first surface presents lower values of displacements, but a more extensive failure surface is found, which encompasses a larger region. On the other hand, the second failure surface presents higher values of displacements, but these are concentrated on the surface face of the analyzed slope. This is because the Cam-Clay Model does not have a cohesion value like the Mohr-Coulomb model.

Knowing that for some soils, the value of the cohesive intercept is a consequence of the overconsolidation of the tested samples, analyzes were carried out to evaluate the effect of the overconsolidation ratio on the *SRF*. This assessment will be detailed in the next item.

4. Sensitivity analysis of the overconsolidation ratio

Complementarily, a sensitivity analysis of the value of the overconsolidation ratio (*OCR*) used in the analysis of shear strength reduction (*SSR*) with the Cam-Clay model was carried out. It is noteworthy that the geometry of the hypothetical slope was changed to reduce the computational cost of the analysis, with the aim of achieving the fastest critical *SRF*, which is illustrated in Figure 13. In the model, 1556 quadrilateral elements were generated with 4 nodes and length of 1 m on the face of the slope and 4 m on the rest of the domain. Boundary conditions were applied that restricted the horizontal displacements on the sides and the vertical displacements on the base of the geometry.

The methodology previously described was applied in a similar manner, where the displacements of six points were monitored, and the *OCR* value was assumed to be 1.00, 1.50, 2.00, 4.00, and 8.00. During the sensitivity analysis, no significant changes in results were observed for overconsolidation ratios

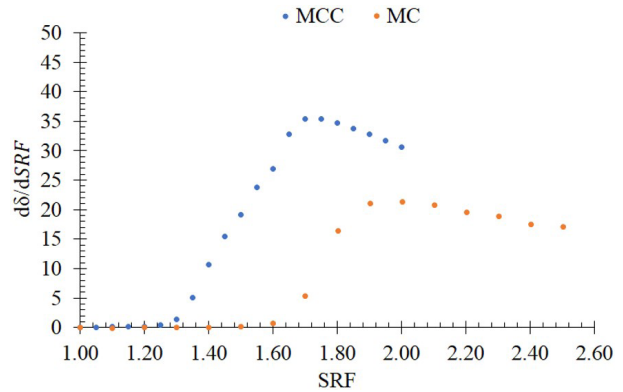


Figure 12. Derivative of each point on the curve of mean displacement values $d\delta / dSRF$ – Comparison between MCC and MC.

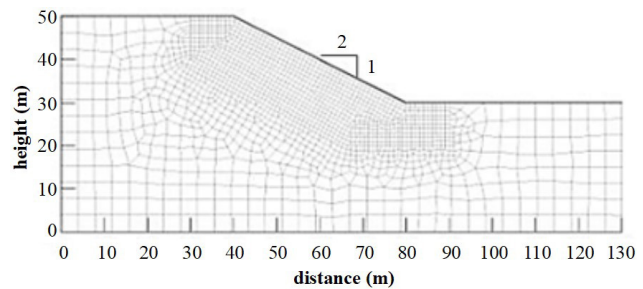


Figure 13. New geometry for overconsolidation ratio sensitivity analysis.

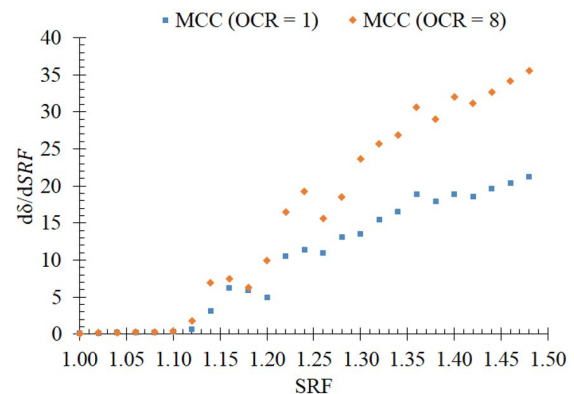


Figure 14. Derivative of each point on the curve of mean displacement values $d\delta / dSRF$ - Comparison between *OCR* = 1 and *OCR* = 8.

greater than one ($OCR > 1$). Therefore, a comparison of results will be presented for *OCR* values of 1, normally consolidated soil, and 8 highly overconsolidated soil.

The value of 1.12 was considered for the critical *SRF* in both cases since the derivative of the mean displacement values of the monitored points as a function of the applied *SRF* indicates an abrupt increase in displacement, an indication of the beginning of rupture (Figure 14).

Figure 15 illustrates the monitored points and indicate the displacements obtained for an *SRF* of 1.12 for normally compacted soil ($OCR = 1$) and pre-consolidated soil ($OCR = 8$).

The failure surface obtained is similar in both cases and the critical *SRF* of 1.12 can also be considered for both cases. However, the pre-consolidated material ($OCR = 8$) showed slightly higher displacement values at the monitored points, one hypothesis would be the different stress paths.

Figure 16 illustrates the difference in the displacement value obtained in both cases for each applied *SRF* value.

In addition, Figure 17 shows the derivative of each point of the displacement curves ($d\delta / dSRF$) illustrated in Figure 16 for values of $OCR = 1$ and $OCR = 8$. It can be observed that the critical *SRF* of 1.12, for the monitored points P1, P2, P3, and P4, can be considered for both normally consolidated material ($OCR = 1$) and overconsolidated material ($OCR = 8$). The points P5 and P6 indicate higher

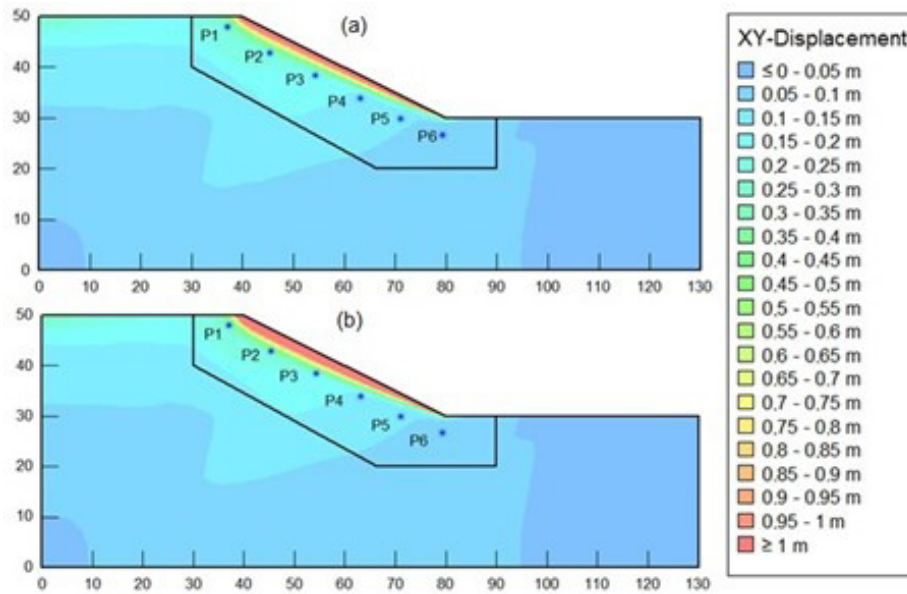


Figure 15. Sensitivity analysis for *SRF* = 1.12, (a) $OCR = 1$ and (b) $OCR = 8$.

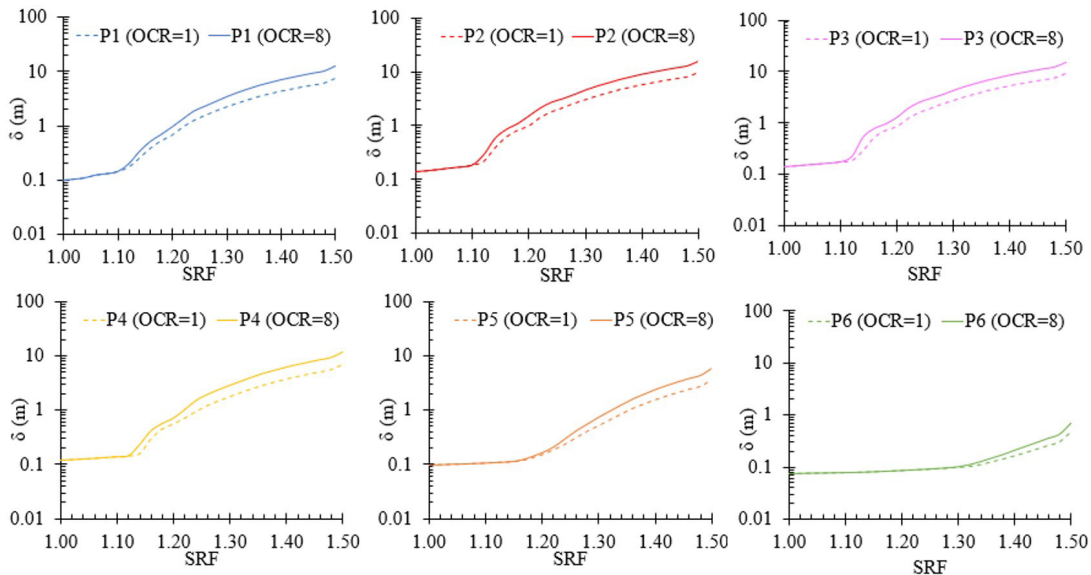


Figure 16. Offset comparison (δ) between $OCR = 1$ and $OCR = 8$.

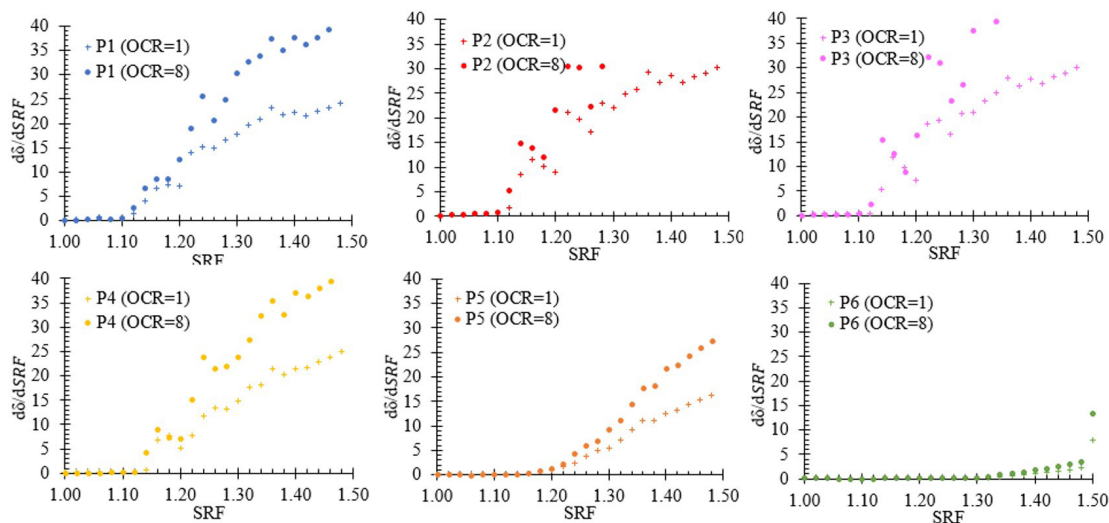


Figure 17. Derivative of each point of the displacement curves $d\delta/dSRF$ - Comparison between $OCR = 1$ and $OCR = 8$.

critical SRF , but they also do not indicate any influence of the OCR value.

One hypothesis that explains the similarity in results is the fact that displacements and SRF depend more on the stress state ($\eta = q/p'$) than on the state parameters p_0 and its variation with increasing SRF . As discussed, points close to the surface would have values of η close to M , and thus, there would be no significant variations in the values of p_0 .

5. Conclusions

The paper presents a discussion about the use of the Critical State Model with hardening when applying the Shear Strength Reduction Method (SSR). Considering the Modified Cam Clay model (MCC), the application of SSR generates a reduction in the slope of the critical state line (CSL) and a variation in the yield surface size. However, the stress state that tends to have the most significant hardening tends to be far from the failure surface, as presented in the MCC model formulation.

The case study presented in this article compared the application of SSR with a perfectly plastic elastic model without hardening with the MCC model, this is a critical state model that considers hardening/softening of the yield surface. The MCC model resulted in a lower SRF value, indicating that the model was more conservative when evaluating the slope stability condition.

Furthermore, an evaluation of the effect of pre-consolidation stress on the SRF was carried out. A similarity in the results was observed for materials with different overconsolidation ratio (OCR) values. One hypothesis that explains this similarity is the fact that the displacements and SRF depend more on the state of stress of the material than on the pre-consolidation stress, a parameter that controls the yield surface size.

For future work, it is suggested to assess the influence of geometry, material strength parameters, dilation angle, material stress state, and to use other constitutive models in order to corroborate the aforementioned hypotheses.

Acknowledgements

The authors would like to thank the Postgraduate Program in Geotechnics of the University of Brasilia and the National Council for Scientific and Technological Development (“CNPq” by Portuguese abbreviation) for the support of this research.

Declaration of interest

The authors have no conflicts of interest to declare. All co-authors have observed and affirmed the contents of the paper and there is no financial interest to report.

Authors’ contributions

Isabella Maria Martins de Souza: conceptualization, data curation, methodology, writing – original draft. Daniela Toro Rojas: conceptualization, writing – original draft. Ana Carolina Gonzaga Pires: validation, writing - reviewing and editing. Márcio Muniz de Farias: validation, reviewing. Manoel Porfirio Cordão Neto: methodology, supervision, validation, writing – review & editing.

Data availability

All data produced or examined in the course of the current study are included in this article.

List of symbols

a_m	Normal to a yield surface
B_{ij}	Matrix that relates displacement and strains
b_m	Normal to the plastic potential function
CSL	Critical State Line
c	Cohesion
D_{ml}	Stress-strain constitutive matrix
D_{ij}^e	Elastic constitutive matrix
D_{ij}^{ep}	Elastic-plastic constitutive matrix
E	Young's Modulus
e_i	Initial void index
F	Yield surface
F_i	External forces
FEM	Finite Element Method
K_{ij}	Stiffness matrix
LEM	Limit Equilibrium Method
	CSL slope in p - q space
MC	Mohr Coulomb
MCC	Modified Cam-Clay Model
η	Stress ratio (q/p')
p'	Mean effective stress
OCR	Overconsolidation ratio
p_0	Preconsolidation stress
q	Deviator stress
SF	Safety Factor
SRF	Strength Reduction Factor
SSR	Shear Strength Reduction
u_j	Displacement vector
Y	Plastic modulus
	Specific weight
δ	Displacement
ε_v^p	Plastic volumetric strain
ν	Poisson Coefficient
ϕ	Friction angle

References

- Cheng, Z., & Jefferies, M. (2020). Implementation and verification of NorSand model in general 3D framework. In *Proceedings of the Geo-Congress 2020: Geotechnical Earthquake Engineering and Special Topics* (pp. 10-19). Reston: ASCE. <https://doi.org/10.1061/9780784482810>.
- Clough, R.W., & Woodward, R. (1967). Analysis of embankment stresses and deformations. *Journal of the Soil Mechanics and Foundations Division*, 4, 529-549. <http://dx.doi.org/10.1061/JSFEAQ.0001005>.
- Dong, L., Wang, J., Li, X., & Peng, K. (2018). Dynamic stability analysis of rockmass: a review. *Advances in Civil Engineering*, 2018, 1-22. <http://dx.doi.org/10.1155/2018/4270187>.
- Duncan, J.M., Wright, S.G., & Brandon, T.L. (2014). *Soil strength and slope stability* (2nd ed.). John Wiley & Sons.
- Farias, M.M., & Naylor, D.J. (1998). Safety analysis using finite elements. *Computers and Geotechnics*, 22(2), 165-181. [http://dx.doi.org/10.1016/S0266-352X\(98\)00005-6](http://dx.doi.org/10.1016/S0266-352X(98)00005-6).
- Fredlund, D.G., & Rahardjo, H. (1993). *Soil mechanics for unsaturated soils*. John Wiley & Sons.
- Fredlund, D.G., & Rahardjo, H. (2012). *Unsaturated soil mechanics in engineering practice*. John Wiley & Sons.
- Futai, M.M. (2002). *Estudo teórico-experimental do comportamento de solos tropicais não-saturados: aplicação a um caso de voçoramento* [Doctoral thesis]. Universidade Federal do Rio de Janeiro (in Portuguese). Geoslope International, Ltd. (2021). *Add-Ins programming guide and reference*. Geoslope International, Ltd.
- Jefferies, M.G. (1993). NorSand: a simple critical state model for sand. *Geotechnique*, 43(1), 91-103. <http://dx.doi.org/10.1680/geot.1993.43.1.91>.
- Jefferies, M.G., & Shuttle, D.A. (2002). Dilatancy in general Cambridge-type models. *Geotechnique*, 52(9), 625-637. <http://dx.doi.org/10.1680/geot.2002.52.9.625>.
- Matsui, T., & San, K. (1992). Finite element slope stability analysis by shear strength reduction technique. *Soil and Foundation*, 32(1), 59-70. <http://dx.doi.org/10.3208/sandf1972.32.59>.
- Roscoe, K.H., & Burland, J.B. (1968). *Engineering plasticity*. Cambridge University Press. On the generalized stress-strain behaviour of wet clay, pp. 535-609.
- Roscoe, K.H., Schofield, A.N., & Wroth, C.P. (1958). On the yielding of soils. *Geotechnique*, 8(1), 22-53. <http://dx.doi.org/10.1680/geot.1958.8.1.22>.
- Roscoe, K.H., Schofield, A.N.D., & Thurairajah, A. (1963). Yielding of clays in states wetter than critical. *Geotechnique*, 13(3), 211-240. <http://dx.doi.org/10.1680/geot.1963.13.3.211>.
- Vardon, P.J., Wang, B., & Hicks, M.A. (2017). Slope failure simulations with MPM. *Journal of Hydrodynamics*, 29(3), 445-451. [http://dx.doi.org/10.1016/S1001-6058\(16\)60755-2](http://dx.doi.org/10.1016/S1001-6058(16)60755-2).